



HAL
open science

Streaming potentials of granular media: Influence of the Dukhin and Reynolds numbers

Alexandre Boleve, Agnès Crespy, André Revil, F. Janod, Jean-Luc Mattiuzzo

► **To cite this version:**

Alexandre Boleve, Agnès Crespy, André Revil, F. Janod, Jean-Luc Mattiuzzo. Streaming potentials of granular media: Influence of the Dukhin and Reynolds numbers. *Journal of Geophysical Research : Solid Earth*, 2007, 112, pp.B08204. 10.1029/2006JB004673 . insu-00403383

HAL Id: insu-00403383

<https://insu.hal.science/insu-00403383>

Submitted on 8 Mar 2021

HAL is a multi-disciplinary open access archive for the deposit and dissemination of scientific research documents, whether they are published or not. The documents may come from teaching and research institutions in France or abroad, or from public or private research centers.

L'archive ouverte pluridisciplinaire **HAL**, est destinée au dépôt et à la diffusion de documents scientifiques de niveau recherche, publiés ou non, émanant des établissements d'enseignement et de recherche français ou étrangers, des laboratoires publics ou privés.

Streaming potentials of granular media: Influence of the Dukhin and Reynolds numbers

A. Bolève,^{1,3} A. Crespy,¹ A. Revil,^{1,2} F. Janod,³ and J. L. Mattiuzzo³

Received 3 August 2006; revised 27 February 2007; accepted 3 May 2007; published 11 August 2007.

[1] Laboratory experiments are performed to understand the controlling parameters of the electrical field associated with the seepage of water through a porous material. We use seven glass bead packs with varying mean grain size in an effort to obtain a standard material for the investigation of these electrical potentials. The mean grain size of these samples is in the range 56–3000 μm . We use pure NaCl electrolytes with conductivity in the range 10^{-4} to 10^{-1} S m^{-1} at 25°C. The flow conditions cover viscous and inertial laminar flow conditions but not turbulent flow. In the relationship between the streaming potential coupling coefficient and the grain size, three distinct domains are defined by the values of two dimensionless numbers, the Dukhin and the Reynolds numbers. The Dukhin number represents the ratio between the surface conductivity of the grains (due to conduction in the electrical double layer coating the surface of the grains) and the pore water electrical conductivity. At high Dukhin numbers ($\gg 1$) and low Reynolds numbers ($\ll 1$), the magnitude of the streaming potential coupling coefficient decreases with the increase of the Dukhin number and depends on the mean grain diameter (and therefore permeability) of the medium. At low Dukhin and Reynolds numbers ($\ll 1$), the streaming potential coupling coefficient becomes independent of the microstructure and is given by the well-known Helmholtz-Smoluchowski equation widely used in the literature. At high Reynolds numbers, the magnitude of the streaming potential coupling coefficient decreases with the increase of the Reynolds number in agreement with a new model developed in this paper. A numerical application is made illustrating the relation between the self-potential signal and the intensity of seepage through a leakage in an embankment.

Citation: Bolève, A., A. Crespy, A. Revil, F. Janod, and J. L. Mattiuzzo (2007), Streaming potentials of granular media: Influence of the Dukhin and Reynolds numbers, *J. Geophys. Res.*, 112, B08204, doi:10.1029/2006JB004673.

1. Introduction

[2] The generation of electrical signals associated with the movement of water in porous/fractured materials is related to the viscous drag of the excess charge contained in the pore water of the porous medium [e.g., *Bull and Gortner*, 1932]. The record of these electrical fields provides a powerful geophysical method for tracking the pattern of groundwater flow. Applications in geohydrology concern the forced movement of water associated with deformation of porous rocks [e.g., *Lorne et al.*, 1999a, 1999b; *Revil et al.*, 2003], the determination of preferential flow paths over karstic areas [*Jardani et al.*, 2006a, 2006b], the determination of transmissive properties of unconfined aquifers [*Titov et al.*, 2000], the determination of subglacial flow patterns [*Kullessa et al.*, 2003a, 2003b], CO₂ sequestration [*Moore et al.*, 2004], and the detection of leakages in embankments and dams and the interpretation of the resul-

ting self-potential signals in terms of seepage velocity [e.g., *Bogoslovsky and Ogilvy*, 1970; *Gex*, 1980; *Panthulu et al.*, 2001; *Sheffer*, 2002; *Sheffer and Howie*, 2001, 2003; *Titov et al.*, 2005; *Rozycki et al.*, 2006]. These works have also recently driven the development of new algorithms of self-potential tomography [e.g., *Revil et al.*, 2001; *Long and Hao*, 2005; *Minsley et al.*, 2007] and tank-scale laboratory measurements in well-controlled conditions to check the underlying physics of these processes [*Maineult et al.*, 2006a, 2006b; *Moore and Glaser*, 2007]. Similar types of analysis were carried out recently in medical imaging to study the flow of electrolytes in cartilage submitted to mechanical loads [*Sachs and Grodzinsky*, 1995; *Garon et al.*, 2002] and in plant sciences to monitor the flow of sap in trees [*Gibert et al.*, 2006].

[3] There are a number of works published in the literature regarding the measurement of streaming potentials associated with the flow of water through granular porous materials [e.g., *Ahmad*, 1964; *Lorne et al.*, 1999a, 1999b; *Guichet et al.*, 2006]. The streaming potential coupling coefficient is a material property arising in the coupled hydroelectric problem of porous material. It represents the variation of the electrical potential to a variation in pore fluid pressure. For example, *Bull and Gortner* [1932] show

¹CNRS-CEREGE, Université Paul Cézanne, IRD, Aix-en-Provence, France.

²Colorado School of Mines, Golden, United States.

³SOBESOL, Savoie Technolac, Le Bourget du Lac Cedex, France.

a decrease of the strength of the streaming potentials by two orders of magnitude when the grain size decreases by two orders of magnitude from ~ 5 to $500 \mu\text{m}$ at low ionic strengths ($\sim 10^{-4}$ N NaCl at 25°C). This decrease was explained by *Revil et al.* [1999b] as resulting from the influence of the surface conductivity of the grains on the streaming potential coupling coefficient in the viscous laminar flow regime.

[4] However, very few researchers have investigated the effect of non-viscous laminar flow upon the electrokinetic process. Streaming potential measurements have been made in capillaries of different radii to see the influence of the viscous sublayer upon the electrokinetic process at high Reynolds numbers [*Bocquet et al.*, 1956; *Kurtz et al.*, 1976]. The Reynolds number is a key-dimensionless number that expresses the ratio of inertial to viscous forces in the Navier-Stokes equation. However, as far as we know, there were no works investigating quantitatively the influence of the Reynolds number upon the value of the streaming potential coupling coefficient at the transition between the viscous-laminar flow regime and the inertial-laminar flow regime in porous media.

[5] In this paper, we propose a new formulation regarding the influence of the Reynolds number upon the coupled hydroelectric problem of porous material. In this formulation, we also account for the influence of surface conductivity of the grains on both the electrical conductivity and the streaming potential coupling coefficient. To check the validity of this model, we measured the streaming potential coupling coefficient and electrical conductivity of glass bead packs at different salinities. We investigate a set of seven well calibrated glass bead packs that can be considered as a standard material for the investigation of electrokinetic phenomena. The mean grain size of each sample is in the range 56 to $3000 \mu\text{m}$ (the permeability of these samples covers approximately four orders of magnitude and the porosity ϕ is approximately that of a random packing of spherical particles, $\phi = 0.40$). We used NaCl solutions with electrical conductivities in the range 10^{-4} to 10^{-1} S m^{-1} at 25°C , corresponding to the conductivity of surface and groundwaters often encountered in nature. Our goal in this paper is to provide a model explaining the variations of the streaming potential with the mean grain diameter of the sample at different salinities. An illustration is made by simulating the intensity of self-potential signals associated with the leakage of water through an embankment. We show that a quantitative relationship exists between the intensity of the self-potential signals and the intensity of seepage.

2. Theoretical Background

[6] In this section, we discuss a theoretical model able to capture the influence of two key dimensionless numbers, namely the Dukhin and the Reynolds numbers, upon the value of the streaming potential coupling coefficient. The streaming potential coupling coefficient is the key parameter that controls the magnitude of self-potential signals associated with the percolation of water through a porous material. This electrokinetic or hydroelectrical phenomenon stems from the existence of an electrical double layer coating the surface of the grains. Indeed, when in contact

with water, the surface of the minerals becomes charged. The fixed charge of the mineral surface is counterbalanced by sorbed charges in the Stern layer plus charges located in the diffuse layer. The counterions correspond to the excess of ions (generally cations) located in the pore space of the porous material. The flow of water through the porous material drags the excess charge contained in the pore space, creating a net source of current density (the streaming current) [e.g., *Lorne et al.*, 1999a, 1999b]. The opposite mechanism exists and corresponds to the flow of pore water in response to the application of an electrical field. This is due to viscous drag of the pore water by the movement of the counterions associated with the application of the electrical field. This mechanism is known as electro-osmosis.

2.1. Viscous Laminar Flow

[7] We consider a granular medium with a narrow particle size distribution centered on a mean particle diameter d_0 . If the distribution of the size of the particles corresponds to a log normal distribution, d_0 corresponds to the peak of this distribution. We denote p the pore fluid pressure (in Pa) and φ the electrical potential (in V). We consider that the pore water is an electrolyte with N ionic species (the mobility of species i is b_i and their charge q_i). The boundary-value problem describing the hydroelectric coupling through a granular porous material is given by the Nernst-Planck and Stokes equations [e.g., *Pride*, 1994; *Revil and Linde*, 2006],

$$\mathbf{j}_f = \sum_{i=1}^N q_i \left[-b_i q_i \bar{C}_i \nabla \varphi + \bar{C}_i \frac{\partial \mathbf{u}_f}{\partial t} \right] \quad (1)$$

$$-\nabla p + \eta_f \nabla^2 \left(\frac{\partial \mathbf{u}_f}{\partial t} \right) + \mathbf{F} = 0, \quad (2)$$

$$\frac{\partial \mathbf{u}_f}{\partial t} = 0, \quad \text{on } S, \quad (3)$$

$$\mathbf{j}_f \cdot \mathbf{n} = 0, \quad \text{on } S \quad (4)$$

where \mathbf{j}_f is the electrical current density in the pore water (in A m^{-2}), $\partial \mathbf{u}_f / \partial t$ is the velocity of the pore fluid (in m s^{-1}) and $\nabla \cdot (\partial \mathbf{u}_f / \partial t) = 0$ (incompressibility of the flow), $\mathbf{F} = -\bar{Q}_V \nabla \varphi$ is the electrostatic microscopic body force per unit volume acting on the pore water, \mathbf{n} is the unit vector normal to the surface of the grains, \bar{Q}_V is the excess charge per unit pore volume (expressed in Coulomb m^{-3}), η_f is the dynamic viscosity of the pore water (in Pa s), and \bar{C}_i is the concentration of species i per unit pore volume. In the following, the pressure will be equal to the hydrostatic fluid pressure (in Pa), $p = \rho_f g h$, where h is the hydraulic head (in m), g is the acceleration due to gravity (in m s^{-2}), and ρ_f is the bulk density of the pore water (in kg m^{-3}).

[8] There are several ways to upscale equations (1) and (2), which are subjected to the local boundary conditions given by equations (3) and (4) plus specified macroscopic boundary conditions. Examples are volume-averaging and differential-effective-medium approaches [see *Pride*, 1994;

Revil, 2002]. In all cases, theories developed in the vicinity of thermodynamic equilibrium yield macroscopic linear constitutive equations between the macroscopic current density \mathbf{J} (in A m^{-2}) and the seepage velocity \mathbf{U} (in m s^{-1}). In the viscous laminar flow regime, this yields,

$$\mathbf{J} = -\sigma(\nabla\phi - C_0\nabla h), \quad (5)$$

$$\mathbf{U} = -K_0\nabla h + C_0\sigma\nabla\phi, \quad (6)$$

where $K_0 = k_0\rho_f g/\eta_f$ is the hydraulic conductivity of the porous medium (in m s^{-1}), k_0 is its permeability (in m^2), σ is the DC-electrical conductivity of the porous material (in S m^{-1}), and C_0 is its streaming potential coupling coefficient, expressed here in volts per meter of hydraulic head and defined by

$$C_0 = \left(\frac{\partial\phi}{\partial h} \right)_{\mathbf{J}=0}. \quad (7)$$

[9] Revil [2002] proposed to use a differential-effective-medium approach to obtain an expression for the electrical conductivity and then for the streaming potential coupling coefficient. This model can be written as [Revil *et al.*, 2002]

$$k_0 = \frac{d_0^2}{\partial F(F-1)^2}, \quad (8)$$

$$C_0\sigma = \rho_f g \frac{\varepsilon_f \zeta}{\eta_f F}, \quad (9)$$

$$\sigma = \sigma_f \xi, \text{ as } \xi \geq 1, \quad (10)$$

$$\sigma = \frac{\sigma_f}{F} \left[F\xi + \frac{1}{2}(1-\xi) \left(1 - \xi + \sqrt{(1-\xi)^2 + 4F\xi} \right) \right], \text{ as } \xi \leq 1, \quad (11)$$

where ε_f is the dielectric constant of water ($\varepsilon_f = 80 \times \varepsilon_0$ where $\varepsilon_0 = 8.84 \times 10^{-12} \text{ F m}^{-1}$ is the dielectric constant of free space), ζ is the so-called zeta potential (a key parameter characterizing the electrical potential of the inner part of the electrical diffuse layer, see Leroy and Revil, 2004), α is an empirical constant [see Revil and Cathles, 1999], $F = \phi^{-m}$ is the electrical formation factor, and σ_f is the electrical conductivity of the brine. The exponent m is often called the cementation exponent or first Archie's exponent, ξ is a dimensionless number called the Dukhin number, the ratio between the surface conductivity of the grains to the electrical conductivity of the pore water [e.g., Shilov *et al.*, 2001]:

$$\xi \equiv \sigma_S/\sigma_f. \quad (12)$$

[10] As shown below, equation (10) is used to capture the non-linear behavior of the relationship between the electrical conductivity of the porous material and the electrical conductivity of the pore water [see discussion in Niwas

et al., 2006]. equations (10) and (11) imply the existence of an iso-conductivity point characterized by $\sigma = \sigma_f = \sigma_S$. At this point, the conductivity of the material is equal to the conductivity of its pore water.

[11] For packing of spheres, the macroscopic surface conductivity σ_S is related to the specific surface conductivity, Σ_S , by [Revil and Linde, 2006],

$$\sigma_S = \frac{6\Sigma_S}{d_0}, \quad (13)$$

where the numerical constant 6 corresponds to spherical grains. Surface conductivity includes conduction in the Stern layer of sorbed counterions and in the diffuse (Gouy-Chapman) layer [Ennis and White, 1996; Revil and Glover, 1997, 1998].

[12] All the material properties entering the constitutive equations depend on only two textural parameters, the mean grain diameter and the formation factor, and two electrical double layer properties, the zeta potential ζ and the specific surface conductivity Σ_S . For simple supporting electrolytes, the zeta potential depends usually on the logarithm of the salinity (and therefore on the logarithm of the electrical conductivity) of the pore water [e.g., Kirby and Hasselbrink, 2004] over a wide range of salinity. Such a dependence was demonstrated theoretically by Revil *et al.* [1999a] using an electrical double layer model. So we can write

$$\zeta = a + b \log_{10} \sigma_f, \quad (14)$$

where a and b are two constants.

[13] The dependence of the specific surface conductivity on salinity is not well known. Most authors consider the surface conductivity to be a constant that is independent of the mineralization and composition of the groundwater. Revil and Glover [1997, 1998], and Leroy and Revil [2004] have proposed double-layer models for silica and aluminosilicates to determine the salinity dependence of surface conductivity. They found that most of the surface conductivity is due to electrical conduction in the Stern layer and that the salinity dependence of the surface conductivity is relatively weak (the situation would be very different if surface conduction occurred mainly in the diffuse Gouy-Chapman layer of counterions). The uncertainty in the electrical conductivity and streaming potential measurements does not allow a salinity dependence of the surface conductivity to be determined so it is customary to assume that surface conductivity is independent of salinity. Because this dependence is probably weak as discussed above, we will adopt this assumption below.

[14] When the Dukhin number is very small, the streaming potential coupling coefficient is given by the Helmholtz-Smoluchowski equation:

$$\lim_{\eta \rightarrow 0} C_0 \equiv C_{HS} = \frac{\varepsilon_f \zeta}{\eta_f \sigma_f}, \quad (15)$$

[15] According to this equation, the streaming potential coupling coefficient is independent of the texture of the porous material and therefore independent of the permeability.

2.2. Inertial Laminar Flow

[16] Darcy's law in its classical form implies a linear relationship between the flux and the gradient of the fluid pressure when the flow is laminar and the viscous (friction) force dominates at the interface between the grains and the pore water. As the Reynolds number increases, we pass from this viscous-laminar flow regime to another laminar flow regime in which the inertial force controls the flow. For a Reynolds number higher than 100–200, flow starts to become turbulent and vorticities appear in the flow lines in the pore space of the material. However, we will not consider the turbulent regime in this paper, as it does not seem to have practical applications in geohydrology of porous media.

[17] *Teng and Zhao* [2000] derived recently a generalized Darcy equation by volume-averaging the local Navier-Stokes momentum equation over a representative elementary volume of a porous material, given by

$$\rho_f \frac{d\mathbf{U}}{dt} + \frac{1+Re}{k_0} \eta_f \mathbf{U} = -\nabla p + \mathbf{F}, \quad (16)$$

where \mathbf{F} is a macroscopic body force and Re is the Reynolds number, a key-dimensionless number that expresses the ratio of inertial to viscous forces in the Navier-Stokes equation [e.g., *Batchelor*, 1972]. For a capillary of radius R , U being the strength of the seepage velocity, the Reynolds number is then defined by [e.g., *Batchelor*, 1972],

$$Re = \frac{\rho_f UR}{\eta_f}. \quad (17)$$

[18] In a porous material, the radius of the capillary should be replaced by a corresponding length scale of the porous material. The Reynolds number is defined by,

$$Re = \frac{\rho_f U \Lambda}{\eta_f}, \quad (18)$$

where Λ is a characteristic length of the flow (for capillaries $\Lambda = R$ where R is the radius of the capillary). If we replace U by the Darcy equation (neglecting the electroosmotic contribution), we can approximate the Reynolds number,

$$Re = \frac{\rho_f^2 g k_0 \Lambda}{\eta_f^2 (1+Re)} \frac{h}{L}, \quad (19)$$

where h is the hydraulic head and L is the length of the cylindrical core pack. For a granular medium with a unimodal particle size distribution, the length scale Λ is given by [*Revil*, 2002]

$$\Lambda = \frac{d_0}{2m(F-1)}. \quad (20)$$

[19] From equations (19) and (20), the Reynolds number is the solution of the following equation,

$$Re^2 + Re - \frac{\rho_f^2 g}{2m\alpha\eta_f^2} \frac{d_0^3}{F(F-1)^3} \left(\frac{h}{L}\right) = 0. \quad (21)$$

[20] The positive root of equation (21) is,

$$Re = \frac{1}{2}(\sqrt{1+c} - 1), \quad (22)$$

$$c = \frac{\beta \rho_f^2 g}{\eta_f^2} \frac{d_0^3}{F(F-1)^3} \left(\frac{h}{L}\right), \quad (23)$$

where $\beta \approx 2.25 \times 10^{-3}$ is a numerical constant (determined from the constants given above). Equation (22) is a new equation that has a strong practical value since it can be easily used to determine the Reynolds number in a porous material from the knowledge of the pressure gradient.

[21] In the present case, the macroscopic body force corresponds to the electrostatic force associated with the excess of electrical charge per unit pore volume. Therefore the generalized Darcy equation, equation (16), can be written as,

$$\mathbf{U} = -\frac{k}{\eta_f} \nabla p - \bar{Q}_V \nabla \varphi, \quad (24)$$

where k is an apparent permeability that is related to the Reynolds number by

$$k/k_0 = 1/(1+Re), \quad (25)$$

$$\lim_{Re \rightarrow 0} k/k_0 = 1, \quad (26)$$

where k is the permeability in viscous laminar flow conditions.

[22] The influence of inertial flow upon electrokinetic coupling has been the subject of very few publications [see recently *Watanabe and Katagishi*, 2006 and references therein]. *Gorelik* [2004] used dimensional analysis to demonstrate that the effect of the Reynolds number corresponds to a multiplication of the Helmholtz-Smoluchowski equation by an unspecified function of the Reynolds number. In this paper, we look for an explicit (quantitative) relationship between the streaming potential coupling coefficient and the Reynolds number. At the scale of a representative elementary volume, the current density is given by [*Revil et al.*, 2005; *Linde et al.*, 2007]

$$\mathbf{J} = -\sigma \nabla \varphi + \bar{Q}_V \mathbf{U}, \quad (27)$$

$$\mathbf{J} = -\sigma \nabla \varphi - \frac{k \bar{Q}_V}{\eta_f} \nabla p, \quad (28)$$

where k is the apparent permeability defined above. The streaming potential coupling coefficient can be related to the excess charge of the diffuse layer per unit pore volume, \bar{Q}_V , by $C_0 = k_0 \bar{Q}_V / \eta_f \sigma$ [*Revil et al.*, 2005]. Equation (27) expresses the fact that the source current density is equal to the excess of charge of the pore fluid \bar{Q}_V times the seepage

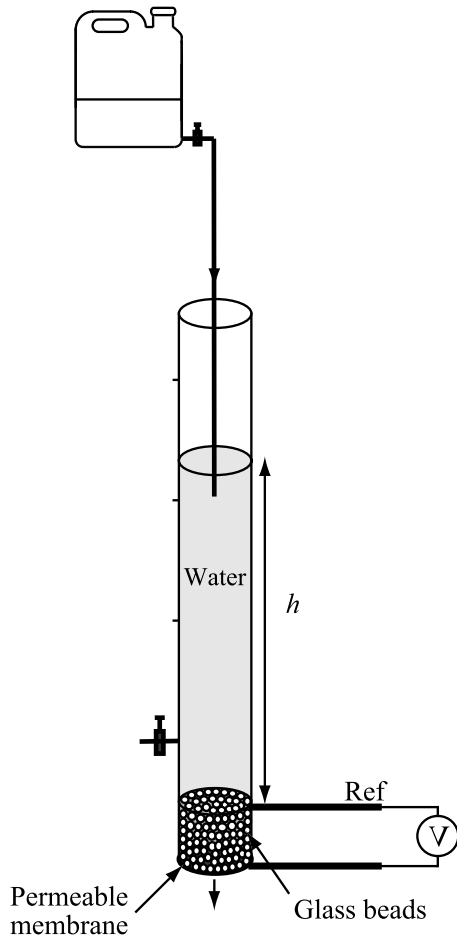


Figure 1. Sketch of the experimental setup. The sample is packed at the bottom of a Plexiglas tube and is maintained in the tube by a permeable membrane with a coarse mesh (the mesh is, however, finer than the diameter of the grains). The record of the self-potentials during the flow of the electrolyte through the sample is done with Ag/AgCl₂ electrodes (“Ref” is the reference electrode). The hydraulic heads are maintained constant at different levels and the streaming potentials are recorded at these levels at the end-faces of the sample.

velocity \mathbf{U} . As the seepage velocity is influenced by the increase of the Reynolds number (for $Re > 0.1$), the Reynolds number also influences the value of the streaming potential coupling coefficient. Following equations (25) and

Table 1. Measured Properties of the Glass Bead Packs

Sample	d range (in μm)	d_0 (in μm)	F^a	σ_S (in mS m^{-1}) ^a	k_0 (in m^2) ^{b c}
S1a	50–60	56	3.3 ± 0.2	0.43 ± 0.05	2.0×10^{-12}
S1b	60–80	72	3.2 ± 0.2	0.32 ± 0.05	3.1×10^{-12}
S2	80–106	93	3.4 ± 0.2	0.26 ± 0.04	4.4×10^{-12}
S3	150–212	181	3.3 ± 0.2	0.13 ± 0.02	2.7×10^{-11}
S4	212–300	256	3.4 ± 0.2	0.08 ± 0.02	5.6×10^{-11}
S5	425–600	512	3.4 ± 0.2	0.05 ± 0.02	1.2×10^{-10}
S6	3000	3000	3.6 ± 0.2	0.10 ± 0.02	1.4×10^{-8}

^aThe uncertainty is determined from the best fit of the electrical conductivity data using equation (11).

^bDetermined from equation (25) where k is the measured value and Re the Reynolds number.

^cThe uncertainty is roughly equal to 10% of the reported value.

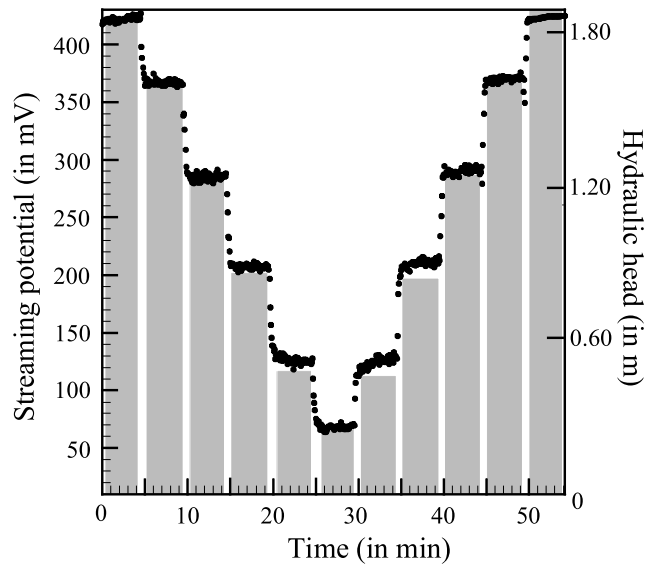


Figure 2. Example of a typical run for sample S3 (grain size of 150–212 μm) and a water conductivity of 10^{-3} S m^{-1} . The filled circles correspond to the measurements of the streaming potential at the two end-faces of the sample while the grey columns correspond to the measurement of the hydraulic heads. The streaming potentials are proportional to the imposed hydraulic heads. The results are reproducible. This means that there is no drift of the electrical potential of the electrodes during the duration of the experiment.

(28), the streaming potential coupling coefficient is related to the Reynolds number by,

$$C/C_0 = 1/(1 + Re), \quad (29)$$

$$\lim_{Re \rightarrow 0} C/C_0 = 1, \quad (30)$$

where C_0 is the streaming potential coupling coefficient in viscous laminar flow conditions and C is the measured coupling coefficient.

[23] In summary, the generalized coupled constitutive equations between the seepage velocity and the electrical current density are,

$$\mathbf{J} = -\sigma \left(\nabla \phi - \frac{C_0}{1 + Re} \nabla h \right), \quad (31)$$

$$\mathbf{U} = -\frac{K_0}{1 + Re} \nabla h + \frac{C_0}{1 + Re} \sigma \Delta \phi, \quad (32)$$

with a preserved symmetry of the coupling term. This means that Onsager’s reciprocity holds. The situation would likely be different in the turbulent flow regime where a magnetic field is probably associated with vortices of the local flow lines in the pore space.

3. Experimental Methods

[24] The experimental setup for the measurement of the streaming potential coupling coefficient is shown in Figure 1a. It consists simply of a Plexiglas tube with a

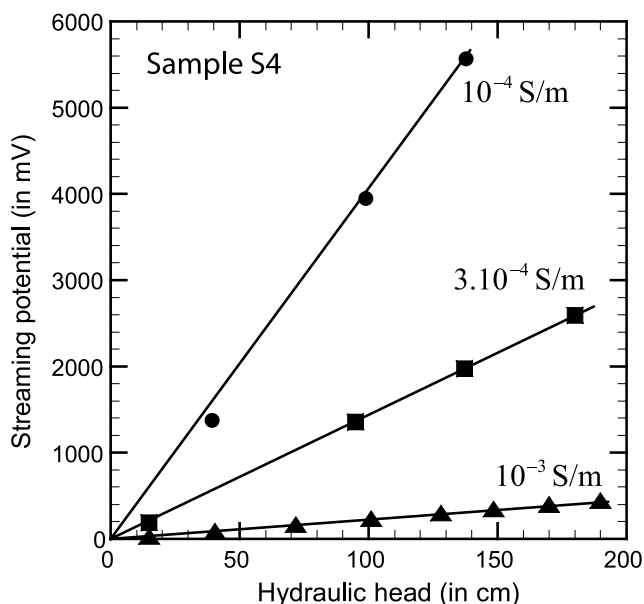


Figure 3. Example of typical runs for sample S4 (grain size of 212–300 μm) at three water conductivities. We observe linear relationships between the variation of the streaming potentials and the variation of the hydraulic heads at these different salinities. At each salinity, the streaming potential coupling coefficient is equal to the slope of the linear trend.

permeable and electrically insulating membrane, placed at its bottom, with a mesh of 50 μm . We check that the permeability of this membrane is always at least ten times larger than the permeability of the sample (for the highly permeable sample S6, we use a coarser mesh). Each sample corresponds to a packing of glass beads (manufactured by Sigma-Aldrich) of a given particle size. They are seven glass bead packs investigated in this study with mean particle size in the range 56–3000 μm , so approximately covering two orders of magnitude in size (Table 1). The chemical composition of the glass is $\text{SiO}_2 \sim 60.5\%$, $\text{Na}_2\text{O} \sim 12$ to 18 %, $\text{CaO} \sim 5$ to 12%, $\text{MgO} \sim 4\%$, $\text{Al}_2\text{O}_3 \sim 1\%$. The measured mass density of the grains is 2430 kg m^{-3} . The measured porosity of the packs is $\phi = 0.40$ irrespective of the size of the glass beads. The other properties of the glass bead packs are reported in Table 1.

[25] To measure the streaming potential coupling coefficient, we use the following protocol. In some cases, a given hydraulic head is imposed on the cylindrical sample inside the tube by adding water to the water column in the tube in such a way that the hydraulic head is maintained constant. We use also for some experiments a falling head method during which the electrical potential is measured during the decrease of the hydraulic head in the tube associated with the flow of the water through the porous pack. The gradient of the fluid pressure is controlled by the hydraulic head in the tube and the length of the porous pack (typically between 1 to 60 centimeters). In both cases, the brine is flowing through the porous sample. The resulting electrical potential is measured with two non-polarizable Ag/AgCl_2 electrodes (Ref321/XR300, Radiometer Analytical) located in the

vicinity of the end faces of the sample. The difference of the electrical potential measured between the end faces of the porous pack divided by the length of the sample is the streaming electrical field associated with the flow of the brine through the pack. The voltages are measured with a data logger (Easy Log, internal impedance of 10 MOhm, sensitivity of 0.1 mV) or with a voltmeter (Metrix MX-20, internal impedance 100 MOhm, sensitivity of 0.1 mV). Both provided consistent measurements.

[26] Streaming potential data from a typical run are shown at Figures 2 and 3. In viscous laminar flow conditions, the differences of the electrical potential measured in the vicinity of the end-faces of the porous medium are proportional to the imposed hydraulic heads, as shown in Figures 2 and 3. The slope of the linear trend of streaming potential vs. head is the streaming potential coupling coefficient, defined from equation (5) by

$$C = \left(\frac{\partial \phi}{\partial h} \right)_{J=0} \quad (33)$$

[27] In addition to the streaming potential coupling coefficient, we determine the intrinsic permeability in viscous-laminar flow conditions by measuring the seepage per unit time at a given hydraulic head (when the flow was not in the viscous-laminar flow regime, we performed a correction using the estimated value of the Reynolds number as explained below). Measurements of the streaming potential coupling coefficient and permeability were performed for different pore water electrical conductivities using different NaCl solutions. These solutions were prepared by measuring the weight of NaCl salt to add to a given solution of deionized water or by measuring directly the conductivity the solution with a calibrated impedancemeter. We use the following set of brine conductivities (3×10^{-2} , 10^{-2} , 3×10^{-3} , 10^{-3} , 3×10^{-4} , and 10^{-4} S m^{-1}) for the streaming potential measurements. The electrical conductivity of the electrolytes was measured with a conductivity meter (CDM-230, MeterLab™). The pH of the solution, measured with the pH-meter (pH-330, SET1-Fisher), is in the range 5.6 to 5.9 at 24.5°C. Values of the streaming potential coupling coefficients are reported in Table 2.

[28] We also measure the electrical conductivity using a frequency-dependent impedancemeter (Waynekerr Analy-

Table 2. Values of the Streaming Potential Coupling Coefficient C_0 (Expressed in mV m^{-1})^a

Sample	3×10^{-2} (S m^{-1})	10^{-2} (S m^{-1})	3×10^{-3} (S m^{-1})	10^{-3} (S m^{-1})	3×10^{-4} (S m^{-1})	10^{-4} (S m^{-1})
S1a	-12.5	-22.0	-75	-159	-454	-647
S1b	-8.5	-36.0	-142	-245	-748	-1944
S2	-8.1	-24.0	-87	-224	-477	-3215
S3	-7.6	-30.5	-137	-319	-1219	-4793
S4	-7.5	-23.0	-82	-317	-1132	-4502
S5	-11.1	-36.0	-107	-331	-1451	-3483
S6	-17.2	-43.0	-159	-510	-1014	-
C_{HS}^b	-6.9	-30.2	-136	-504	-2033	-7063

^aThe coefficient C_0 is determined from equation (29) where C is the measured coupling coefficient and Re is the Reynolds number determined using equation (22) (Measurements made at $25 \pm 1^\circ\text{C}$).

^bValues predicted by the Helmholtz-Smoluchowski equation (in mV/m).

Table 3. Measurements of the Electrical Conductivity of the Samples σ (in 10^{-4} S m^{-1}) as a Function of the Electrical Conductivity of the Solution

Sample	10^{-1} (S m^{-1})	6×10^{-2} (S m^{-1})	3×10^{-2} (S m^{-1})	10^{-2} (S m^{-1})	3×10^{-3} (S m^{-1})	10^{-3} (S m^{-1})	3×10^{-4} (S m^{-1})	10^{-4} (S m^{-1})
S1a	289.5	199.0	100.9	38.4	12.61	6.59	3.38	2.11
S1b	291.4	199.0	101.3	38.6	12.30	6.62	2.54	1.94
S2	291.4	195.6	91.6	32.6	11.77	6.20	2.29	1.78
S3	290.9	193.0	86.8	32.7	11.74	5.11	1.81	1.19
S4	288.0	188.7	86.5	31.9	11.47	3.78	1.33	1.08
S5	283.1	187.3	84.6	31.5	11.14	3.31	1.14	0.94
S6	279.8	182.0	75.6	31.6	9.61	3.59	2.28	0.91

ser 6425) in the frequency range 30 Hz–300 kHz. Electrical conductivity measurements were performed in the frequency domain with a two-electrode device (with stainless steel electrodes) according to the protocol described in *Revil et al.* [2002]. We use the following set of brine conductivities (10^{-1} , 6×10^{-2} , 3×10^{-2} , 10^{-2} , 3×10^{-3} , 10^{-3} , 3×10^{-4} , and 10^{-4} S m^{-1}) for the electrical conductivity measurements. The description of this protocol will not be repeated here. Accuracy of the measurement is estimated to be 5%. Values of the electrical conductivity are reported in Table 3. They are obtained at a frequency of a few hundreds of Hertz to a few kHz.

[29] Permeability is determined using Darcy's law and measuring the volume of water passing through the glass packs per unit time. Measurements were reproducible with an uncertainty of 10%. Values of the measured intrinsic permeability (in the viscous laminar flow regime) are reported in Table 1.

4. Results and Discussion

4.1. Intrinsic Permeability

[30] In Figure 4, we plot the measured intrinsic permeabilities versus the intrinsic permeabilities predicted by equation (8) corrected for the influence of the Reynolds number (see equations (22) and (25)). There is very good agreement between the measured data and the prediction of equation (8).

4.2. Electrical Conductivity

[31] In Figure 5, we plot the electrical conductivity of the samples as a function of the electrical conductivity of the pore water. We use equation (11) to fit these experimental data in order to determine the value of the surface conductivity and the electrical formation factor. The mean formation factor is 3.4 ± 0.1 (see Table 1). Using Archie's law, $F = \phi^{-m}$ and a porosity of 0.40, we obtain a cementation exponent $m = 1.34$ (this is consistent with the cementation exponent of unconsolidated sands and glass beads reported by *Sen et al.* [1981]).

[32] The value of surface conductivity of each pack is reported as a function of the mean diameter of each pack in Figure 6. We see very clearly that surface conductivity is inversely proportional to the mean diameter of the beads as predicted by the theory. The value of the specific surface conductivity obtained from this trend, $\Sigma_S = 4.0 \times 10^{-9}$ S, is consistent with the double layer model prediction of *Revil et al.* [1999a] for a salinity of 10^{-3} S m^{-1} , and with previous experimental data [*O'Brien and Rowlands*, 1993]. Other estimates of the specific surface conductance are reported in Table 4. They are consistent with the above estimate.

Brovelli et al. [2005] used a finite element code to simulate electrical conduction in a partially water-saturated sandstone. They obtained $\Sigma_S = 3.3 \times 10^{-7}$ S. *Wildenschild et al.* [2000] obtained Σ_S in the range $(0.5-1.5) \times 10^{-7}$ S using electrical conductivity data on mixtures of sand and clay particles. *Block and Harris* [2006] found $\Sigma_S = 4.2 \times 10^{-8}$ S with sand with a small amount of clay particles. However, none of these authors discussed the discrepancy between their estimates and those obtained from electrical triple layer calculations [see *Revil and Glover*, 1997, 1998; *Revil and Leroy*, 2001; *Leroy and Revil*, 2004]. Our conclusion is that the values derived by *Wildenschild et al.* [2000], *Brovelli et al.* [2005], and *Block and Harris* [2006] are strongly overestimated by one to two orders of magnitude because of the inappropriate mean grain size used by these authors to estimate the surface conductance from the macroscopic surface conductivity.

[33] The “conductivity ratio” of the porous samples is defined as the ratio between the electrical conductivity of the porous pack to the conductivity of the brine. These conductivity ratios are plotted in Figure 7 as a function of the Dukhin numbers for all the samples. As discussed by *Revil et al.* [2002], this provides a way to normalize electrical conductivity plots. We observe that all the data fall on the same curve that is well reproduced by our model. This shows the power of our electrical conductivity model to represent accurately the electrical conductivity response

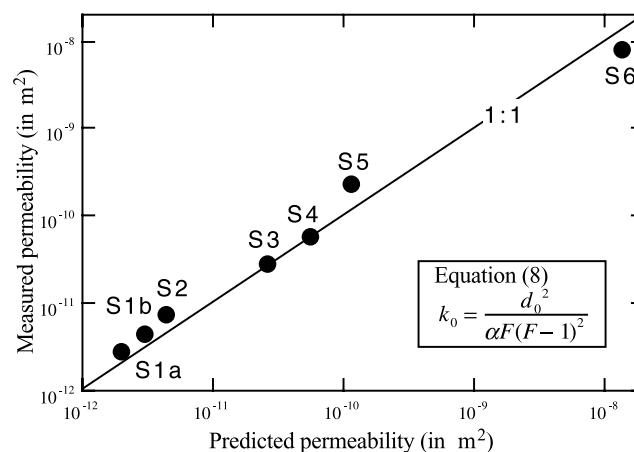


Figure 4. Measured versus modeled intrinsic permeability for the samples investigated in this study. We use $\alpha = 53$, and the formation factor is equal to 3.4. For sample S6, the measured permeability is corrected for the value of the Reynolds number using the formulae given in the main text, equations (22) and (25).

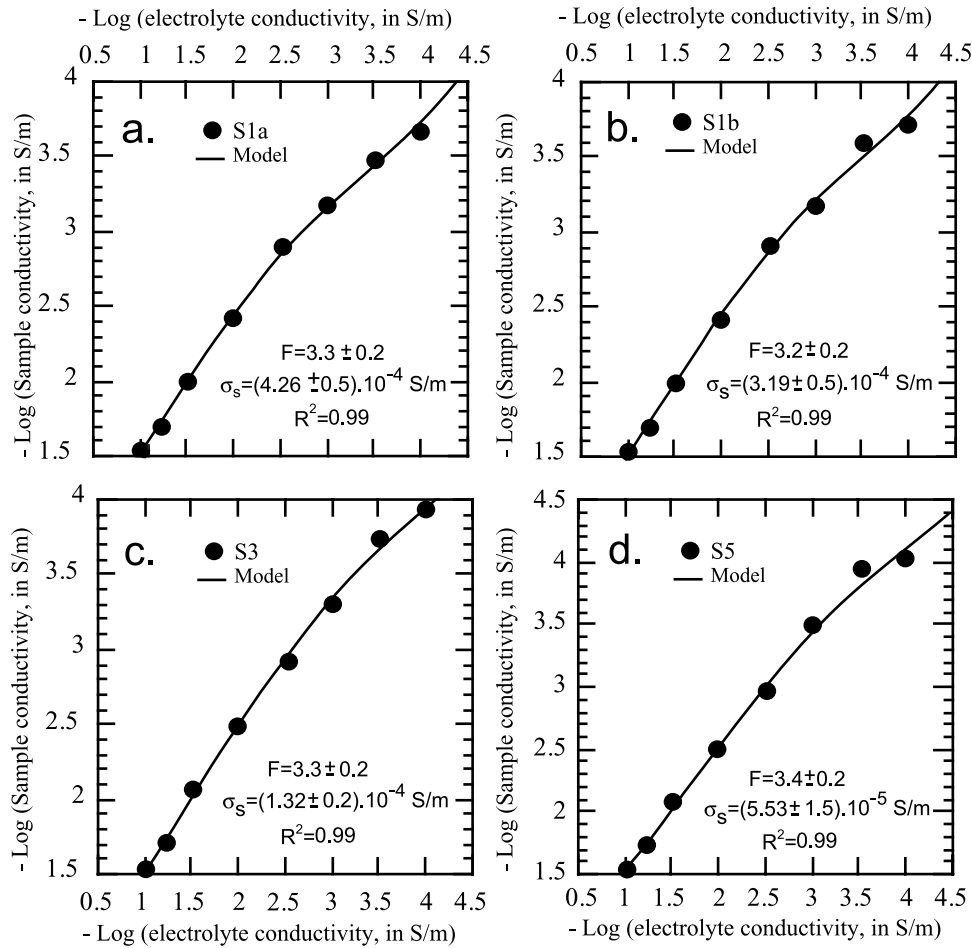


Figure 5. Plots showing the logarithm of the electrical conductivity of four samples σ versus the logarithm of the electrical conductivity of the brine σ_f . The iso-conductivity point is defined by the condition $\sigma = \sigma_f$ for which we also have $\sigma_s = \sigma_f$. The surface conductivity σ_s and the electrical formation factor F are inverted from equation (11) and the experimental data. The plain lines represent the best fit of the model. Note the very good agreement between the model and the experimental data.

of granular materials. We point out that popular electrical conductivity models such as the *Waxman and Smits* [1968] model [or all the family of “linear conductivity models”, see *Niwas et al.*, 2006] cannot reproduce these experimental data as they do not explain the occurrence of an iso-conductivity point.

4.3. Coupling Coefficient

[34] The model developed for the streaming potential coupling coefficient in Section 2 can be summarized by the following equation,

$$C = C_{HS} \frac{G(Re)}{H(\xi)}, \quad (34)$$

where $G(Re) = 1/(1 + Re)$ and $H(\xi) = F\sigma_0(\xi)/\sigma_f$. In this section, we test the accuracy of Equation (34) to determine the streaming potential coupling coefficient and therefore to demonstrate that the coupling coefficient is controlled by the Dukhin and Reynolds numbers.

[35] A preliminary step is to determine the dependence of the zeta potential on the conductivity of the pore water as

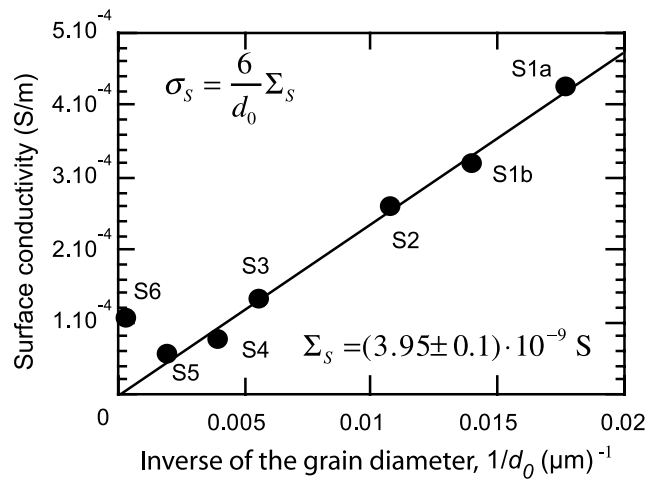


Figure 6. Surface conductivity σ_s versus the inverse of the mean bead size. The linear trend is used to determine the specific surface conductivity, which is equal to $\Sigma_s = 4.0 \times 10^{-9}$ S. Note the excellent correlation between the surface conductivity data and the mean diameter of the beads in the packs (except for sample S6), in agreement with the theory.

Table 4. Surface Conductivity, Grain Size Relationship (NaCl Solutions) (S: Silica, GB: Glass Beads)

Study	Material	σ_s (in 10^{-4} S m^{-1})	d_0 (in μm)	σ_f (in S m^{-1})	T (in $^{\circ}C$)	pH	Σ_s (in $10^{-9}S$)
<i>Bull and Gortner</i> [1932] (using measurements of the streaming potential coupling coefficient).	S-NaCl	71 ± 4	4.5	2.4×10^{-3}	24.5	5.7	5.3
<i>Lorne et al.</i> [1999a] (using measurements of the electrical conductivity).	S-KCl	1.03 ± 0.04	80	10^{-4}	25.0	5.7	1.4
<i>Watanabe and Katagishi</i> [2006] (using measurements of the electrical conductivity).	GB-NaCl	1.3 ± 0.1	115	10^{-4}	23.0	7.5	2.5

discussed in Section 2. Using equation (9), we combined the measurements of the streaming potential coupling coefficient and the measurements of the electrical conductivity to determine the values of the zeta potential in viscous-laminar flow conditions. The results are reported as a function of the logarithm of the electrical conductivity of the pore water in Figure 8. These results are consistent with the values usually reported for silica and glasses [e.g., Kirby and Hasselbrink, 2004]. The constants a and b of equation (14) corresponding to the best fit of the zeta-potential values are reported in Figure 8. With the values of a and b and equation (14), we can estimate the value of the streaming potential coupling coefficient via the Helmholtz-Smoluchowski equation at a given electrical conductivity

of the pore water. These values are reported in the last line of Table 2.

[36] We first check the relationship between the streaming potential coupling coefficient and the Dukhin number ξ . In Figure 9, we plot the reduced streaming potential coupling coefficient C_0/C_{HS} versus the Dukhin number for the seven packs. The measured value of the streaming potential coupling coefficient C , determined from equation (33), is corrected for the influence of the Reynolds number using equations (29) and (22). Note that because the formation factor is roughly the same for all the samples, all the data fall on the same curve. There is a good match between the theory and the experimental data (see Figure 9).

[37] Finally, we check the relationship between both the streaming potential coupling coefficient and the Reynolds number Re . In Figure 10, we plot the reduced streaming potential coupling coefficient C/C_0 (where $C_0 = C_{HS}/H(\xi)$,

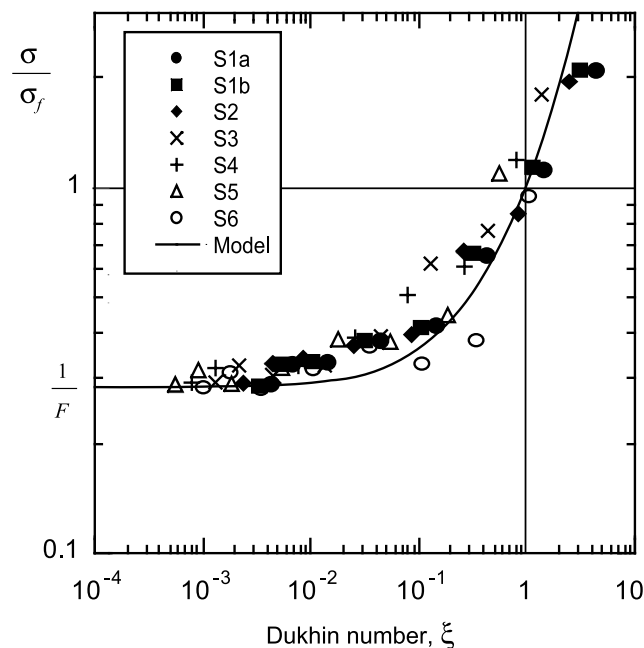


Figure 7. Reduced conductivity ratio σ/σ_f versus the Dukhin number ξ for all the glass bead packs investigated in this study (F is the electrical formation factor). The curve corresponds to the electrical conductivity model discussed in the main text, equation (11). Note the existence of an iso-conductivity point, (1, 1) in the coordinates of the plot. Note that the existence of this iso-conductivity point is not predicted by classical models like the *Waxman and Smits* [1968] formula.

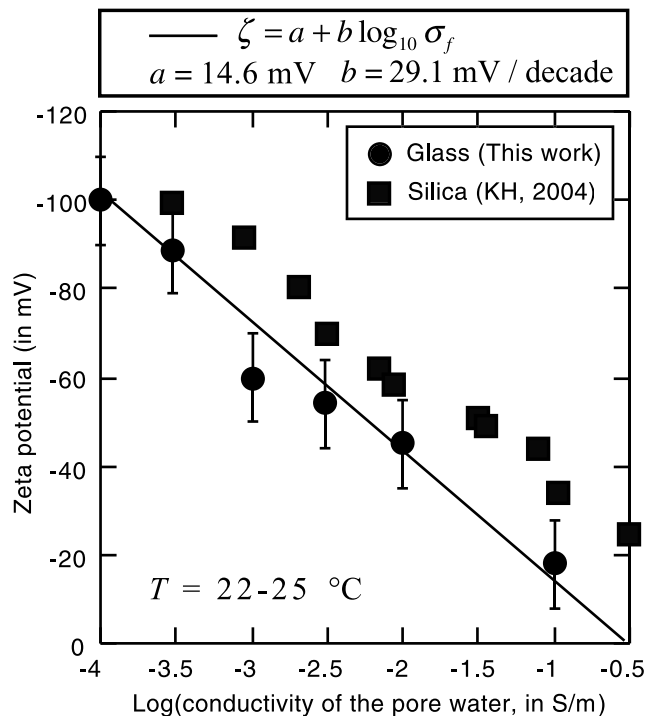


Figure 8. Zeta potential (in mV) versus the logarithm of the electrical conductivity of the pore water ($r = 0.95$) (NaCl, pH 5.6–5.9, 24 $^{\circ}C$). For comparison, we include the data reported for silica by Kirby and Hasselbrink (KH, 2004) (NaCl, pH 7, 25 $^{\circ}C$).

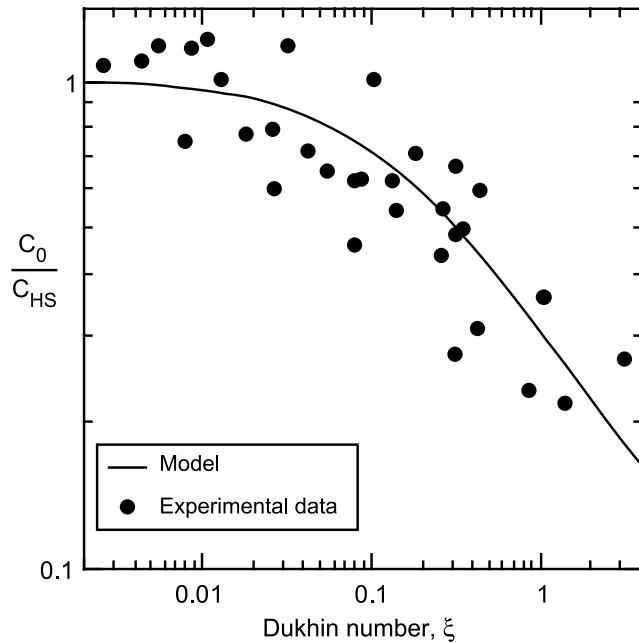


Figure 9. Reduced streaming potential coupling coefficient C_0/C_{HS} versus the Dukhin number ξ (determined from the measured surface conductivity divided by the conductivity of the brine) for all the samples investigated in this study (see Table 2). Note that because the formation factor is roughly the same for all the samples, all the data fall on the same trend. The curve corresponds to the model discussed in the main text.

F) and the reduced permeability k/k_0 versus the Reynolds number for the seven samples investigated in this study. All the data fall on the same curve. The curves correspond to equation (33) for the ratio C/C_0 . Again, we found a good agreement between the theory and the experimental data. It is clear from these data that the decrease of the streaming potential coupling coefficient with the increase of the Reynolds number is entirely due to the increase of the flow rate in the sample during the transition from viscous- to inertial-laminar flows. However, the situation could be different for turbulent flow.

[38] We can summarize our findings in the following way. At high Dukhin numbers ($\gg 1$) and low Reynolds numbers ($\ll 1$), the magnitude of the streaming potential coupling coefficient decreases with the increase of the Dukhin number and depends on the mean grain diameter (and therefore permeability) of the medium. At low Dukhin and Reynolds numbers ($\ll 1$), the streaming potential coupling coefficient becomes independent of the microstructure and is given by the well-known Helmholtz-Smoluchowski equation widely used in the literature. At high Reynolds numbers, the magnitude of the streaming potential coupling coefficient decreases with the increase of the Reynolds number in agreement with the new model developed in section 2.

[39] A recent paper by *Kuwano et al.* [2006] investigated how the apparent permeability and the apparent streaming current coupling coefficient depend on the Reynolds number like in the present work. These authors realized experiments showing a decrease of the streaming current coupling coefficient L and permeability k of glass bead packs with the

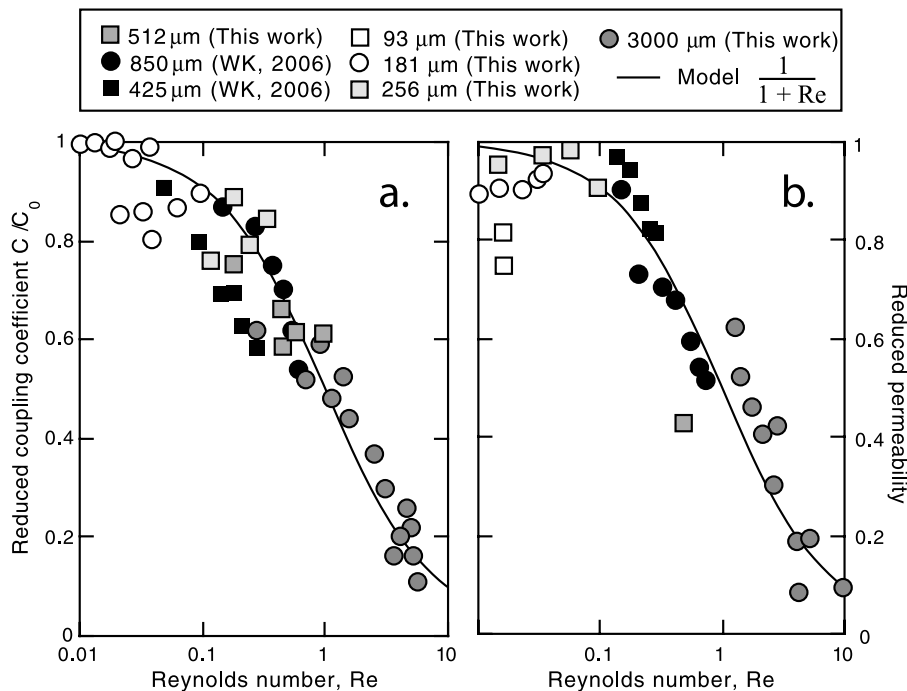


Figure 10. Influence of the Reynolds number determined from equations (22) and (23), upon the relative coupling coefficient C/C_0 (where C is the measured apparent streaming potential coupling coefficient and C_0 is given by equation (15)) and the relative permeability k/k_0 (where k is the measured apparent permeability (using Darcy’s law) and k_0 is given by equation (8)). These measurements have been made at different salinities showing the universal character of this trend.

Table 5. Value of the Variables Used to Compute the Self-Potential Response to the Seepage Flow Through the Pipe

Property	Symbol	Value	Units
Length of the pipe	L_p	8.5	m
Diameter of the pipe	d	0.15	m
Length of the basin	L	34.5	m
Width of the basin	l	21	m
Height of the basin	h	3.5	m
Water conductivity	σ_f	3.7×10^{-2}	S m^{-1}
Clay conductivity	σ_c	5.8×10^{-2}	S m^{-1}
Gravel conductivity	σ_g	1.3×10^{-2}	S m^{-1}
Gravel EK current coefficient	L_g	7.75×10^{-9}	$\text{A m}^{-1} \text{Pa}^{-1}$

Reynolds number Re . They also noted qualitatively that L decreases less than k with Re and suggested that this difference could be related to the increase in the efficiency of charge transport in the vicinity of the surface of the minerals when the Reynolds number increases. This effect could reflect a change in the shape of the velocity profile of the water in the pores when the Reynolds number increases. According to *Revil* [2007], the data presented by *Kuwano et al.* can be fitted with the following parametric function $L(Re) = L_0 (1 + Re)^{-n}$ where $n = 1/2$. Additional investigations will be performed to test this point further.

5. Example of Geophysical Application

[40] The modified form of the constitutive equations described above can be applied to the study of electromagnetic signals associated with fracturing (see the recent paper by *Moore and Glaser, 2007*, this field will be explored in a future contribution) and to the study of leakage in embankments and dams. In this section, we simulate a leakage problem. The geometry of the basin in which the leakage occurs is shown in Figure 3. Previous simulations of such hydroelectric problem were mainly 2D and were not accounting for the influence of the Reynolds number [see *Wilt and Corwin, 1989; Titov et al., 2000, 2005* and references therein and recently *Suski et al., 2006*]. In this paper, we use the finite element code *Comsol Multiphysic 3.2* to simulate the 3D distribution of the self-potential signals associated with the leakage of water through a highly permeable pipe located in the wall of the basin. Dimensions of the pool are reported in Table 5. The basin is assumed to be filled with water with an electrical conductivity equal to $3.7 \times 10^{-2} \text{ S m}^{-1}$ (at 20°C). We assume that the material used for the basin is a clay material. The pipe is filled with the gravel with a formation factor equal to 2.9 and an intrinsic permeability equal to $k_0 = 4.6 \times 10^{-9} \text{ m}^2$. Because of the strong contrast of permeability between the material filling the pipe and the clay, the leakage of water occurs mainly through the pipe.

[41] *Comsol Multiphysic 3.2* is first used to solve the continuity equation $\nabla \cdot \mathbf{U} = 0$ with appropriate boundary conditions for the pressure head in the basin and equation (32) for the Darcy velocity and neglecting electro-osmosis. At the entrance of the pipe, we impose the seepage velocity according to the modified Darcy's law that account for the Reynolds number, equation (32) where h/L is the hydraulic gradient and L is now equal to the length of the pipe and h is the total

hydraulic head (including the length of the pipe), k_0 is the permeability of the gravel filling the pipe. At the exit of pipe, we also imposed the flux that is conservative (in steady state conditions), assuming therefore no exchange of water between the pipe and the surrounding clay material. Therefore the magnitude of the seepage velocity at the entrance of the pipe is equal to the magnitude of the seepage velocity of the exit of the pipe. For all other boundary conditions, we have no flux (only a given head).

[42] For the electrical problem, we solve the continuity equation for the electrical charge $\nabla \cdot \mathbf{J} = 0$ combined with equation (31). This lead to a Poisson's equation for the electrical potential with a source term depending on the distribution of the fluid pressure [e.g., *Titov et al., 2000* and *2005* and references therein]. The values of the electrical conductivity of three materials (tap water, clay, and gravel), voltage and current coupling coefficients and dimensions of the system are reported in Table 5. At the outer boundaries of the basin, we use $\mathbf{n} \cdot \nabla \varphi = 0$ as an appropriate boundary condition (contact with an insulating body like the atmosphere). A reference for the voltage is placed at a reference station chosen arbitrarily in the basin but far enough from the leaking pipe (see "Ref" in Figure 11).

[43] Figures 12 and 13 show the distribution of the equipotentials for the self-potential in the pool (for $k_0 = 4.6 \times 10^{-9} \text{ m}^2$). The leakage is clearly associated with a negative self-potential anomaly centered on the area of

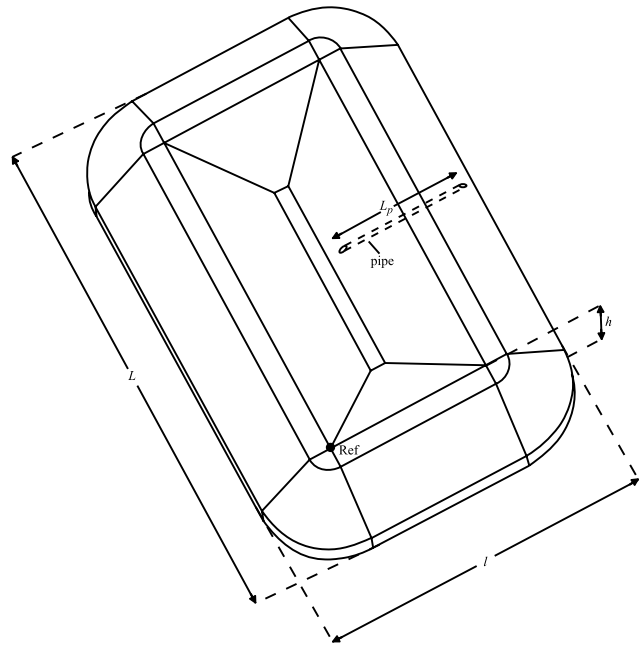


Figure 11. Geometry of water-filled basin with the position of the gravel-filled pipe, which constitutes the preferential fluid flow pathways for the water. The embankment is made of clay (permeability 10 mD , 10^{-14} m^2). The reference for the electrical potential (position of the reference electrode where the electrical potential is taken equal to zero) is placed at the point Ref (ideally it should be located as far as possible from the self-potential anomaly resulting from the pipe).

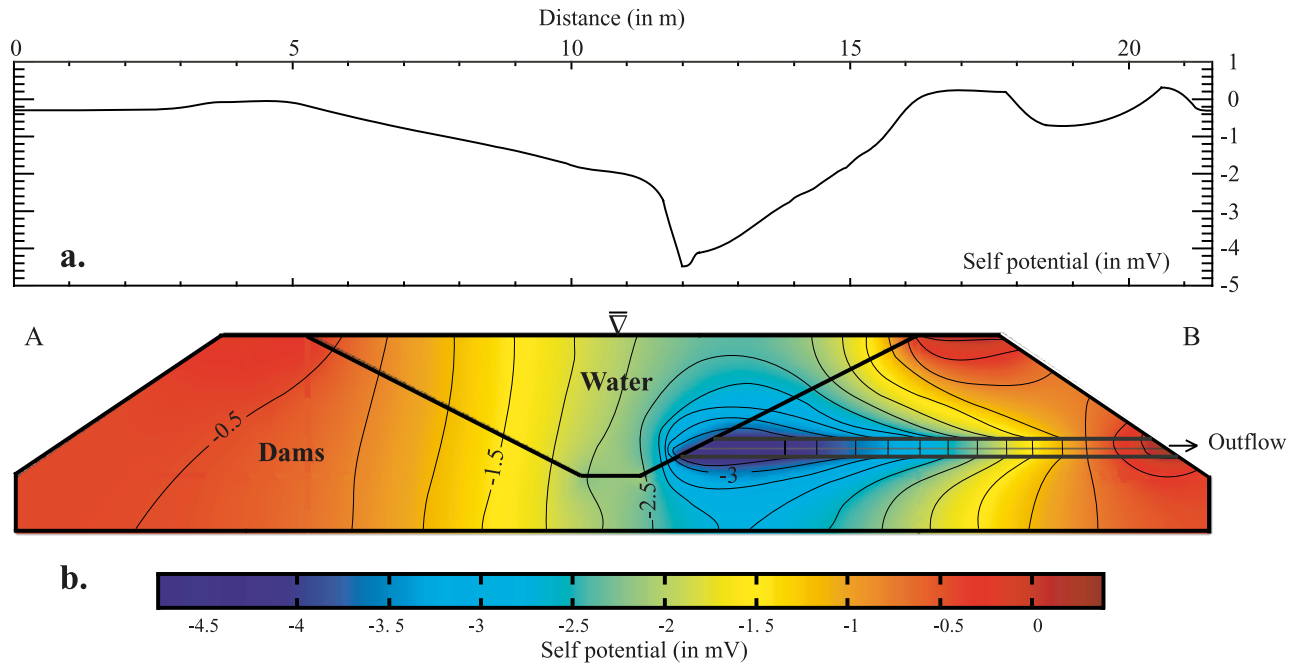


Figure 12. Plot showing the distribution of the electrical potential along a cross-section parallel to the pipe (the reference for the self-potential signals is shown in Figure 4). (a) Distribution at the surface of the dams. The minimum of the self-potential distribution is located at the entrance of the pipe where a negative self-potential anomaly is observed (with an amplitude of few mV). Note that in water, the sensitivity of the measurements is typically 0.2 mV, which warrants a good signal-to-noise ratio. (b) Distribution of the streaming equipotentials.

leakage in agreement with field observations [e.g., Bogoslovsky and Ogilvy, 1970; Sheffer, 2002; Sheffer and Howie, 2001, 2003]. The magnitude of this anomaly at the entrance of the pipe is equal to four millivolts. This anomaly can be well resolved using filtering analysis and a sensitive voltmeter (e.g., the Metrix MX20 has a sensitivity of 0.1 mV). Simulations indicate that applying our model for poorly mineralized water (e.g., 10^{-3} S m^{-1} at 20°C), the intensity of the self-potential anomaly can reach very easily 100 mV.

[44] To test the evolution of a self-potential anomaly associated with the evolution of a leaking area, we modeled the intensity of the self-potential anomaly resulting from an increase of the intrinsic permeability k_0 over time. In this case, the model shows a decrease of the maximum of the self-potential anomaly when the intrinsic permeability increases (Figure 14). This variation is due to the decrease of the streaming potential coupling coefficient with the Reynolds number. There is clearly a domain of intrinsic permeability for which the magnitude of the self-potential anomaly can be used to retrieve the magnitude of the seepage velocity. The self-potential method could be also combined with other methods (e.g., thermal methods) to improve its ability to determine the seepage velocity of leaking areas though joint inversion of self-potential and temperature measurements.

6. Concluding Statements

[45] In this paper, we show how the streaming potential coupling coefficient depends non-linearly on two key

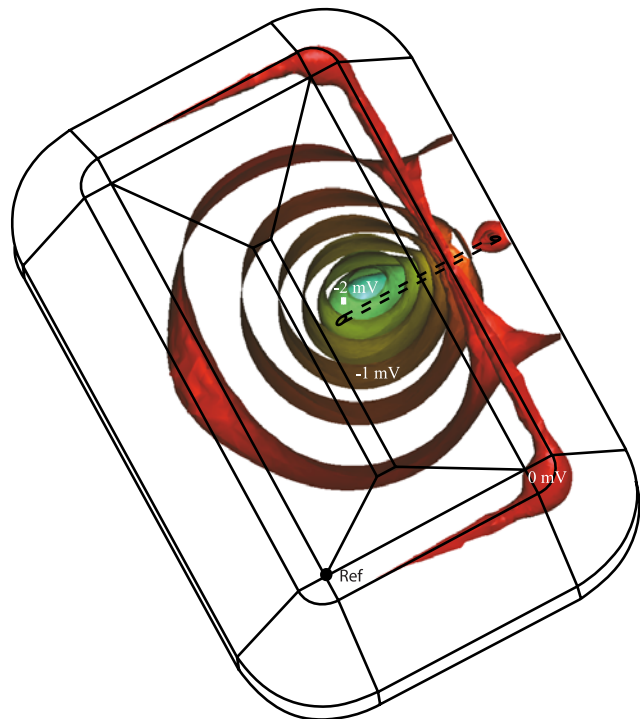


Figure 13. 3D-distribution of the electrical equipotentials in the basin due to the leakage of water through the pipe. The maximum intensity of the self-potential anomaly is 4 mV at the entrance of the leaking area.

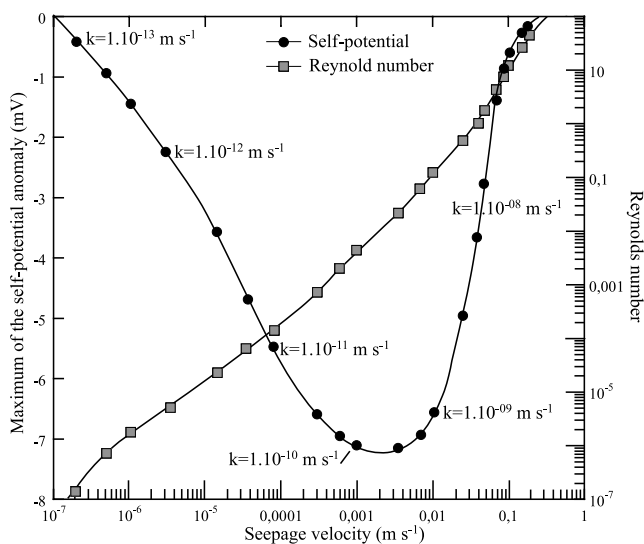


Figure 14. Maximum of the self potential anomaly at the entrance of the pipe versus the seepage velocity for different value of intrinsic permeability k_0 . When the intrinsic permeability k_0 increases over time, there is a decrease of the magnitude of the self-potential anomaly due to the increase of the Reynolds number.

dimensionless parameters, the so-called Dukhin and Reynolds numbers. The Dukhin number characterizes the relative influence of the surface conductivity of the grains (which depends on the grain size) to the conductivity of the pore water electrolyte. The Reynolds number characterizes the influence of the inertial force in the Navier-Stokes equation. In this paper, we have derived (i) a new expression for the Reynolds number and (ii) a general equation for the streaming potential coupling coefficient showing that the Helmholtz-Smoluchowski equation is recovered when both the Reynolds and the Dukhin numbers are much smaller than unity, that is, when viscous-laminar flow and pore water conduction dominate. In the transition between the viscous and inertial laminar flow regimes, the streaming potential coupling coefficient falls as $1/(1 + Re)$ with the increase of the Reynolds number. In addition, (iii) a new set of experimental data has been obtained and both these data and the model agree with each other. Finally (iv) for the first time, we show how surface conductivity varies with the size of the grains. We show that the value of the specific surface conductance agrees with that predicted by double-layer models. Finally, we show that our model can easily be incorporated in finite element simulation software to determine the intensity of self-potential signals associated with leakage. We expect application of this theory also for the potential breaking of seals in the context of CO_2 sequestration.

[46] Extension of the present work will concern mixtures of beads with different grain sizes and clay-bead mixtures, the study of heterogeneities with glass bead packs in series and in parallel, and the application of the present work to real rocks. However, we believe that we can already apply the present petrophysical model to the determination of the relationship between the seepage velocity and the self-potential anomalies measured in various environments and especially in geohydrology to interpret quantitatively self-

potential anomalies related to leakage of water in embankments and dams for example [e.g., Sheffer and Howie, 2001, 2003] and to fracturing in active volcanoes [e.g., Revil et al., 2003; Finizola et al., 2004].

[47] **Acknowledgments.** This work is supported by ANR Project ERINOH in France related to the study of leakages in embankments dams and ANR-ECCO-PNRH Project POLARIS. The Ph-D Thesis of A. Bolève is supported by SOBESOL and the Ph-D thesis of Agnès Crespy by the Ministère de la Recherche et de l'Enseignement in France.

References

- Ahmad, M. (1964), A laboratory study of streaming potentials, *Geophys. Prospect.*, *12*, 49–64.
- Batchelor, G. K. (1972), *An Introduction to Fluid Dynamics*, Cambridge University Press.
- Block, G. I., and J. G. Harris (2006), Conductivity dependence of seismic-electric wave phenomena in fluid-saturated sediments, *J. Geophys. Res.*, *111*, B01304, doi:10.1029/2005JB003798.
- Bocquet, P. E., C. M. Slipevich, and D. F. Bohr (1956), Effects of turbulence on the streaming potential, *Ind. Eng. Chem.*, *48*, 197–200.
- Bogoslovsky, V. A., and V. A. Ogilvy (1970), Natural potential anomalies as a quantitative index of the role of water seepage from reservoir, *Geophys. Prospect.*, *18*, 261–268.
- Brovelli, A., G. Cassiani, E. Dalla, F. Bergamini, D. Pitea, and A. M. Binley (2005), Electrical properties of partially saturated sandstones: novel computational approach with hydrogeophysical applications, *Water Resour. Res.*, *41*, W08411, doi:10.1029/2004WR003628.
- Bull, H. B., and R. A. Gortner (1932), Electrokinetic potentials. X. The effect of particle size on potentials, *J. Phys. Chem.*, *36*, 111–119.
- Ennis, J., and L. R. White (1996), Dynamic Stern layer contribution to the frequency-dependent mobility of a spherical colloid particle: A low-zeta-potential analytic solution, *J. Colloid Interface Sci.*, *178*(2), 446–459.
- Finizola, A., J. F. Lénat, O. Macedo, D. Ramos, J. C. Thouret, and F. Sortino (2004), Fluid circulation and structural discontinuities inside Misti volcano (Peru) inferred from self-potential measurements, *J. Volcanol. Geotherm. Res.*, *135*(4), 343–360.
- Garon, M., A. Légaré, R. Guardo, P. Savard, and M. D. Buschmann (2002), Streaming potentials maps are spatially resolved indicators of amplitude, frequency and ionic strength dependant responses of articular cartilage to load, *J. Biomechanics*, *35*(2), 207–216.
- Gex, P. (1980), Electrofiltration phenomena associated with several dam sites, *Bull. Soc. Vaud Sci. Nature*, *357*(75), 39–50.
- Gibert, D., J.-L. Le Mouél, L. Lambs, F. Nicollin, and F. Perrier (2006), Sap flow and daily electrical potential variations in a tree trunk, *Plant Sci.*, *171*(5), 572–584.
- Gorelik, L. V. (2004), Investigation of dynamic streaming potential by dimensional analysis, *J. Colloid Interface Sci.*, *274*, 695–700.
- Guichet, X., L. Jouniaux, and N. Catel (2006), Modification of streaming potential by precipitation of calcite in a sand-water system: laboratory measurements in the pH range from 4 to 12, *Geophys. J. Int.*, *166*(1), 445–460.
- Jardani, A., J. P. Dupont, and A. Revil (2006a), Self potential signals associated with preferential groundwater flow pathways in sinkholes, *J. Geophys. Res.*, *111*, B09204, doi:10.1029/2005JB004231.
- Jardani, A., A. Revil, F. Akoa, M. Schmutz, N. Florsch, and J. P. Dupont (2006b), Least-squares inversion of self-potential (SP) data and application to the shallow flow of the ground water in sinkholes, *Geophys. Res. Lett.*, *33*(19), L19306, doi:10.1029/2006GL027458.
- Kirby, B. J., and E. F. Hasselbrink (2004), Zeta potential of microfluidic substrates. 1. Theory, experimental techniques, and effects on separations, *Electrophoresis*, *25*, 187–202.
- Kulesa, B., B. Hubbard, and G. H. Brown (2003a), Cross-coupled flow modeling of coincident streaming and electrochemical potentials, and application to subglacial self-potential (SP) data, *J. Geophys. Res.*, *108*(B8), 2381, doi:10.1029/2001JB001167.
- Kulesa, B., B. Hubbard, G. H. Brown, and J. Becker (2003b), Earth tide forcing of glacier drainage, *Geophys. Res. Lett.*, *30*(1), 1011, doi:10.1029/2002GL015303.
- Kurtz, R. J., E. Findl, Al. B. Kurtz, and L. C. Stormo (1976), Turbulent flow streaming potentials in large bore tubing, *J. Colloid Interface Sci.*, *57*, 28–39.
- Kuwano, O., M. Nakatani, and S. Yoshida (2006), Effect of the flow state on streaming current, *Geophys. Res. Lett.*, *33*, L21309, doi:10.1029/2006GL027712.
- Leroy, P., and A. Revil (2004), A triple layer model of the surface electrochemical properties of clay minerals, *J. Colloid Interface Sci.*, *270*(2), 371–380.

- Linde, N., D. Jougnot, A. Revil, S. K. Matthai, T. Arora, D. Renard, and C. Doussan (2007), Streaming current generation in two-phase flow conditions, *Geophys. Res. Lett.*, *34*(3), L03306, doi:10.1029/2006GL028878.
- Long, H. L., and J. Q. Hao (2005), Theoretical and experimental research on self-potential tomography, *Chin. J. Geophys. – Chinese Edition*, *48*(6), 1343–1349.
- Lorne, B., F. Perrier, and J. P. Avouac (1999a), Streaming potential measurements 1. Properties of the electrical double layer from crushed rock samples, *J. Geophys. Res.*, *104*, 17,857–17,877.
- Lorne, B., F. Perrier, and J. P. Avouac (1999b), Streaming potential measurements 2. Relationship between electrical and hydraulic patterns from rock samples during deformation, *J. Geophys. Res.*, *104*, 17,879–17,896.
- Maineult, A., Y. Bernabé, and P. Ackerer (2006a), Detection of advected concentration and pH fronts from self-potential measurements, *J. Geophys. Res.*, *110*(B11), B11205, doi:10.1029/2005JB003824.
- Maineult, A., Y. Bernabé, and P. Ackerer (2006b), Detection of advected, reacting redox fronts from self-potential measurements, *J. Contam. Hydrol.*, *86*(1–2), 32–52.
- Minsley, B. J., J. Sogade, and F. D. Morgan (2007), Three-dimensional source inversion of self-potential data, *J. Geophys. Res.*, *112*, B02202, doi:10.1029/2006JB004262.
- Moore, J. R., and S. D. Glaser (2007), Self-potential observations during hydraulic fracturing, *J. Geophys. Res.*, *112*, B02204, doi:10.1029/2006JB004373.
- Moore, J. R., S. D. Glaser, H. F. Morrison, and G. M. Hoversten (2004), The streaming potential of liquid carbonate dioxide in Berea sandstone, *Geophys. Res. Lett.*, *31*(17), L17610, doi:10.1029/2004GL020774.
- Niwas, S., P. K. Gupta, and O. A. L. de Lima (2006), Nonlinear electrical response of saturated shaley sand reservoir and its asymptotic approximations, *Geophysics*, *71*(3), G129–G133.
- O'Brien, R. W., and W. N. Rowlands (1993), Measuring the Surface Conductance of Kaolinite Particles, *J. Colloid Interface Sci.*, *159*(2), 471–476.
- Panthulu, T. V., C. Krishnaiah, and J. M. Shirke (2001), Detection of seepage paths in earth dams using self-potential and electrical resistivity methods, *Eng. Geol.*, *59*, 281–295.
- Revil, A. (2002), The hydroelectric problem of porous rocks: thermodynamic approach and introduction of a percolation threshold, *Geophys. J. Int.*, *151*(3), 944–949.
- Revil, A. (2007), Comment on “Effect of the flow state on streaming current” by O. Kuwano, M. Nakatani, and S. Yoshida, *Geophys. Res. Lett.*, *34*, L09311, doi:10.1029/2006GL028806.
- Revil, A., and L. M. Cathles (1999), Permeability of shaly sands, *Water Resour. Res.*, *35*(3), 651–662.
- Revil, A., and P. W. J. Glover (1997), Theory of ionic surface electrical conduction in porous media, *Phys. Rev. B.*, *55*(3), 1757–1773.
- Revil, A., and P. W. J. Glover (1998), Nature of surface electrical conductivity in natural sands, sandstones, and clays, *Geophys. Res. Lett.*, *25*(5), 691–694.
- Revil, A., and P. Leroy (2001), Hydroelectric coupling in a clayey material, *Geophys. Res. Lett.*, *28*(8), 1643–1646.
- Revil, A., and N. Linde (2006), Chemico-electromechanical coupling in microporous media, *J. Colloid Interface Sci.*, *302*, 682–694.
- Revil, A., P. A. Pezard, and P. W. J. Glover (1999a), Streaming potential in porous media. 1. Theory of the zeta-potential, *J. Geophys. Res.*, *104*(B9), 20,021–20,031.
- Revil, A., H. Schwaeger, L. M. Cathles, and P. Manhardt (1999b), Streaming potential in porous media. 2. Theory and application to geothermal systems, *J. Geophys. Res.*, *104*(B9), 20,033–20,048.
- Revil, A., L. Ehouame, and E. Thyreault (2001), Tomography of self-potential anomalies of electrochemical nature, *Geophys. Res. Lett.*, *28*(23), 4363–4366.
- Revil, A., D. Hermitte, E. Spangenberg, and J. J. Cochémé (2002), Electrical properties of zeolitized volcanoclastic materials, *J. Geophys. Res.*, *107*(B8), 2168, doi:10.1029/2001JB000599.
- Revil, A., G. Saracco, and P. Labazuy (2003), The volcano-electric effect, *J. Geophys. Res.*, *108*(B5), 2251, doi:10.1029/2002JB001835.
- Revil, A., P. Leroy, and K. Titov (2005), Characterization of transport properties of argillaceous sediments, Application to the Callovo-Oxfordian Argillite, *J. Geophys. Res.*, *110*, B06202, doi:10.1029/2004JB003442.
- Rozycki, A., J. M. R. Fonticella, and A. Cuadra (2006), Detection and evaluation of horizontal fractures in Earth dams using self-potential method, *Engineering Geology*, *82*(3), 145–153.
- Sachs, J. R., and A. J. Grodzinsky (1995), Electromechanical spectroscopy of cartilage using a surface probe with applied mechanical displacement, *J. Biomechanics*, *28*(8), 963–976.
- Sen, P. N., C. Scala, and M. H. Cohen (1981), A self-similar model for sedimentary rocks with application to the dielectric constant of fused glass beads, *Geophysics*, *46*(5), 781–795.
- Sheffer, M. R. (2002), Response of the self-potential method to changing seepage conditions in embankments dams, M. A.Sc. Thesis, Dept. of Civil Eng., University of British Columbia, April 2002.
- Sheffer, M. R., and J. A. Howie (2001), Imaging subsurface seepage conditions through the modeling of streaming potential, Proceedings of 54th Canadian Geotechnical Conference, Calgary, P. 1094–1101.
- Sheffer, M. R., and J. A. Howie (2003), A numerical modelling procedure for the study of the streaming potential phenomenon in embankment dams, Symposium on the Application of Geophysics to Engineering and Environmental Problems, San Antonio, p. 475–487.
- Shilov, V. N., A. V. Delgado, F. Gonzalez-Caballero, and C. Grosse (2001), Thin double layer theory of the wide-frequency range dielectric dispersion of suspensions of non-conducting spherical particles including surface conductivity of the stagnant layer, *Colloids Surf. A: Physicochem. Eng. Aspect.*, *192*, 253–265.
- Suski, B., A. Revil, K. Titov, P. Konosavsky, M. Voltz, C. Dagès, and O. Huttel (2006), Monitoring of an infiltration experiment using the self-potential method, *Water Resour. Res.*, *42*, W08418, doi:10.1029/2005WR004840.
- Teng, H., and T. S. Zhao (2000), An extension of Darcy's law to non-Stokes flow in porous media, *Chem. Eng. Sci.*, *55*, 2727–2735.
- Titov, K., Loukmanov, and A. Potapov (2000), Monitoring of water seepage from a reservoir using resistivity and self-polarization methods: case history of the Petergoph fountain water supply system, *First Break*, *18*, 431–435.
- Titov, K., A. Levitski, P. K. Konosavski, A. V. Tarasov, Y. Ilyin, and M. A. Buès (2005), Combined application of surface geoelectrical methods for groundwater flow modeling: a case history, *Geophysics*, *70*(5), H21–H31.
- Watanabe, T., and Y. Katagishi (2006), Deviation of linear relation between streaming potential and pore fluid pressure difference in granular material at relatively high Reynolds numbers, *Earth Planets Space*, *58*(8), 1045–1051.
- Waxman, M. H., and L. J. M. Smits (1968), Electrical conductivity in oil-bearing sands, *J. Soc. Petrol. Eng.*, *8*, 107–122.
- Wildenschild, D., Roberts, and E. Carlberg (2000), On the relationship between microstructure and electrical and hydraulic properties of sand-clay mixtures, *Geophys. Res. Lett.*, *27*(19), 3085–3088.
- Wilt, M. J., and R. F. Corwin (1989), Numerical modeling of self-potential anomalies due to leaky dams: Model and field examples. In: *Lecture Notes in Earth Sciences*, vol. 27, ed. G. P. Merkle et al., Detection of subsurface flow phenomena, Springer-Verlag, Berlin Heidelberg; 73–89.

A. Bolève, A. Crespy, and A. Revil, CNRS-CEREGE, Université Paul Cézanne, IRD, Aix-en-Provence, France. (revil@cerege.fr)

F. Janod and J. L. Mattiuzzo, SOBESOL, Savoie Technolac, BP 230, F-73375, Le Bourget du Lac Cedex, France.